Nanoscale Res Lett (2009) 4:888–895
DOI 10.1007/s11671-009-9331-9

NANO EXPRESS

Pulsed-Laser-Induced Simple Synthetic Route for $Tb_3Al_5O_{12}:Ce^{3+}$ Colloidal Nanocrystals and Their Luminescent Properties

Sung Wook Mhin · Jeong Ho Ryu · Kang Min Kim · Gyeong Seon Park · Han Wool Ryu · Kwang Bo Shim · Takeshi Sasaki · Naoto Koshizaki

Received: 11 March 2009 / Accepted: 24 April 2009 / Published online: 15 May 2009

Abstract Cerium-doped $Tb_3Al_5O_{12}$ ($TAG:Ce^{3+}$) colloidal nanocrystals were synthesized by pulsed laser ablation (PLA) in de-ionized water and lauryl dimethylaminoacetic acid betain (LDA) aqueous solution for luminescent bio-labeling application. The influence of LDA molecules on the crystallinity, crystal morphology, crystallite size, and luminescent properties of the prepared $TAG:Ce^{3+}$ colloidal nanocrystals was investigated in detail. When the LDA solution was used, smaller average crystallite size, narrower size distribution, and enhanced luminescence were observed. These characteristics were explained by the effective role of occupying the oxygen defects on the surface of $TAG:Ce^{3+}$ colloidal nanocrystal because the amphoteric LDA molecules were attached by positively charged $TAG:Ce^{3+}$ colloidal nanocrystals. The blue-shifted phenomena found in luminescent spectra of the $TAG:Ce^{3+}$ colloidal nanocrystals could not be explained by previous crystal field theory. We discuss the 5d energy level of Ce^{3+} with decreased crystal size with a phenomenological model that explains the relationship between bond distance with 5d energy level of Ce^{3+} based on the concept of crystal field theory modified by covalency contribution.

Keywords $TAG:Ce^{3+}$ nanocrystal · Pulsed laser ablation · LDA · Luminescence · Blue-shift

S. W. Mhin · K. B. Shim
Division of Materials Science and Engineering, Hanyang University, 17 Haengdang-Dong, Seongdong-Gu, Seoul 133-791, South Korea

J. H. Ryu (✉) · G. S. Park
LED Lab, R&D Institute, Samsung LED Co., Ltd., 314, Maetan3-Dong, Yeongtong-Gu, Suwon, Gyunggi-Do 443-743, South Korea
e-mail: jimihen.ryu@samsung.com

K. M. Kim
The Institute of Scientific and Industrial Research, Osaka University, Ibaraki, Osaka 567-0047, Japan

H. W. Ryu
eMD Center, Samsung Electro-Mechanics Co., Ltd., 314, Maetan3-Dong, Yeongtong-Gu, Suwon, Gyunggi-Do 443-743, South Korea

T. Sasaki · N. Koshizaki
High Interface Area Nanostructure Group, Nanotechnology Research Institute (NRI), National Institute of Advanced Industrial Science and Technology (AIST), Tsukuba Central 5, 1-1-1 Higashi, Tsukuba, Ibaraki 305-8565, Japan

Introduction

Integrated sensors for biological application and a variety of molecular-sensing schemes characterized by electrochemistry, refractive index, UV absorption, and luminescence have been devised in an effort to understand the spatio-temporal interplay of biomolecules in biology [1–4]. In particular, luminescent labeling for cellular imaging and assay detection is a standard technique used to understand the interaction of biomolecules in biology [5–7]. However, organic dyes, luminescent proteins or lanthanide chelates as bio-labeling agents may cause problems such as broad spectrum profiles, low photo-bleaching thresholds, and poor photochemical stability.

Ce^{3+}-doped terbium aluminum garnet ($Tb_3Al_5O_{12}:Ce^{3+}$, $TAG:Ce^{3+}$), which has been widely used as a white solid-state light emitting device, may be an alternative label to overcome these problems because of its chemical and thermal stability [8]. We believe that $TAG:Ce^{3+}$ nanocrystal can be substituted for chalcogenide phosphor

as a bio-label for several reasons. Not only does TAG:Ce^{3+} have the potential to obtain luminescent quantum efficiency up to 40% by the allowed 4f → 5d transition of Ce^{3+}, but it is also considered as a nontoxic material [9]. In addition, in the in vivo experiment, the cells are not degraded by blue light, the excitation source for emission from TAG:Ce^{3+}.

Generally, the conventional solid-state reaction method has been used to fabricate TAG:Ce^{3+} crystal. However, this method requires a relatively long processing time and temperature over 1500 °C to obtain single-phase product. Moreover, there have been few reports on the preparation of nano-sized TAG:Ce^{3+} crystals [10]. Under these circumstances, a novel preparation method for TAG:Ce^{3+} nanocrystal would be greatly valuable. One novel technique for synthesizing TAG:Ce^{3+} nanocrystals is pulsed laser ablation (PLA) in liquid media. This technique provides remarkable advantages: simplicity in the synthesis process, the availability of various liquid media, and the absence of chemical reagents in solution [11–13]. Moreover, PLA is a convenient technology for synthesize nanostructured materials, and some researchers have made achievements on this research field [14–16].

In general, luminescence efficiency of phosphor materials goes down with diminution of crystallite size into nanometer range, because an increase in surface-to-volume ratio seriously induces nonradiative processes related to surface defects. In our previous report, Ce^{3+}-doped yttrium aluminum garnet (YAG:Ce^{3+}) nanoparticles were successfully fabricated by laser ablation in de-ionized water [17]. However, luminescence efficiency was considerably low compared to bulk target, which were due to increased surface defects. Therefore, it is necessary to cap such defects by an appropriate surfactant to enhance luminescence efficiency. In this work, we report a new synthetic approach to directly produce highly dispersed and strongly luminescent TAG:Ce^{3+} colloidal nanocrystals for application to luminescent bio-labeling by PLA in aqueous solution. Moreover, the change of 5d electron energy level of Ce^{3+} in nanoscaled TAG crystal, which has attracted much discussion in recent years [18, 19], was investigated in detail.

Experimental

A cerium 3 mol% doped TAG:Ce^{3+} target ($(Tb_{1-x}Ce_x)_3Al_5O_{12}$, $x = 0.03$) was fabricated by spark plasma sintering (SPS) method at 1400 °C for 5 min. The fabricated TAG:Ce^{3+} target was fixed in the bottom of a glass vessel containing 5 mL high-purity de-ionized water and solution of lauryl dimethylaminoacetic acid betaine (LDA, 10^{-2} mol/L) as an amphoteric surfactant. Although a number of surfactants are widely used in laser ablation process, the LDA have been reported to lead to smaller average size and narrow distribution, as well as enhanced emission intensity [20]. The fixed target was irradiated by a Nd:YAG pulse laser (repetition rate of 30 Hz, pulse width of 5–7 ns, maximum output of 60 mW) with the third harmonic wavelength (355 nm). The laser was focused on a spot 1 mm in diameter on the TAG:Ce^{3+} target with a focal length of 250 mm. The target was rotated during laser ablation to avoid deep ablation traces by continuous irradiation of the laser beam. Laser ablation of the TAG:Ce^{3+} target was carried out for 1 h at room temperature. Figure 1 illustrates the laser ablation process in liquid medium for preparation of TAG:Ce^{3+} nanocrystals.

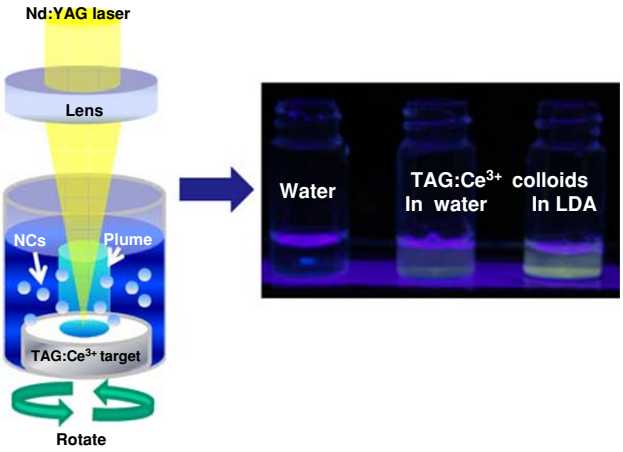

Fig. 1 Schematic diagrams representing PLA of target in liquid medium. The insets illustrate TAG:Ce^{3+} colloidal suspensions prepared by PLA in de-ionized water and LDA solution for 1 h excited by an UV lamp

The colloidal suspension was dropped on a copper mesh coated with amorphous carbon film to observe the microstructure and shape of nanocrystals by a transmission electron microscope (JEOL JEM-2010). The size of the nanocrystals was statistically analyzed using 160 nanoparticles in an TEM image. The precipitates of colloidal suspension were repeatedly centrifuged at 30,000 rpm by an ultracentrifuge (Hitachi CS100GXL) for the X-ray diffraction (XRD, Rigaku RAD-C, Cu $K\alpha$ radiation) and X-ray photoelectron spectroscopy (XPS, Perkin-Elmer PHI-5600ci) measurement. The binding energy was determined with reference to the C 1s line at 184.6 eV of adventitious carbon. Standard atomic concentration calculation provided content of doped Ce atoms in the colloidal nanocrystals. Luminescence spectra of the TAG:Ce^{3+} nanocrystal-dispersed suspensions were measured using a fluorescence spectrometer (PerkinElmer LS-45) at room temperature. The excitation wavelength used for measuring emission spectra was 460 nm, and the excitation spectra were measured at emission maxima.

Results and Discussion

Synthesis of TAG:Ce^{3+} Colloidal Nanocrystals

Figure 2 shows XRD patterns of the TAG:Ce^{3+} nanocrystals collected from colloidal suspensions prepared by PLA in (a) de-ionized water and (b) LDA solution. Bragg reflection peaks of the nanocrystals corresponded to the cubic structured TAG:Ce^{3+} without any peaks assigned to Tb_2O_3, Al_2O_3, $TbAlO_3$, or $Tb_2Al_4O_9$ phases. The TAG:Ce^{3+} nanocrystals formed in de-ionized water had some amorphous phase. However, in the case of LDA solution, the broad amorphous component was diminished and crystallinity was improved compared to the case of de-ionized water.

The crystal morphology, crystal size, and crystallinity were observed more closely by TEM. Figure 3 represents typical TEM micrographs of TAG:Ce^{3+} colloidal nanocrystal prepared by PLA in (a) de-ionized water and (b) LDA solution with corresponding electron diffraction patterns. The morphology of the nanocrystals prepared in de-ionized water (a) indicated that spherical aggregates coexisted with dispersed spherical nanocrystals. Corresponding selected area electron diffraction (SAED) patterns revealed diffused characteristic ring patterns, which confirmed the presence of an amorphous phase. Compared to the case of de-ionized water, smaller, and more highly dispersed TAG:Ce^{3+} nanocrystals were obtained in LDA solution as shown in Fig. 3(b). The SAED patterns of TAG:Ce^{3+} colloidal nanocrystal prepared in LDA solution as shown in inset of Fig. 3(b) revealed bright polycrystalline diffraction rings,

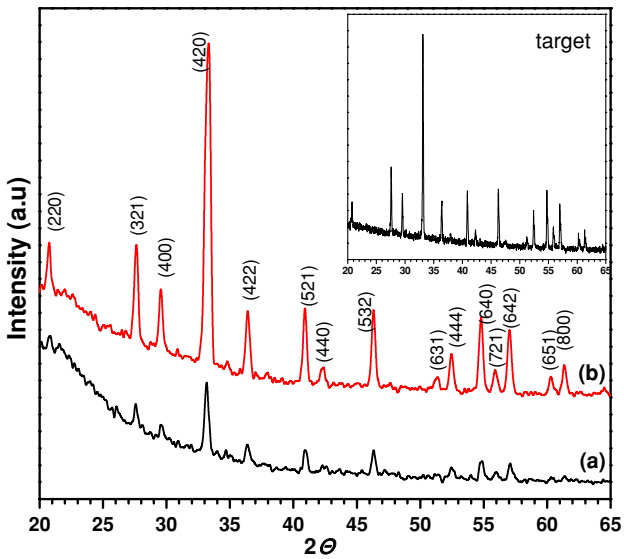

Fig. 2 XRD patterns of the TAG:Ce^{3+} nanocrystals prepared by PLA in **a** de-ionized water and **b** LDA solution. The inset depicts the XRD pattern of TAG:Ce^{3+} bulk target fabricated by SPS

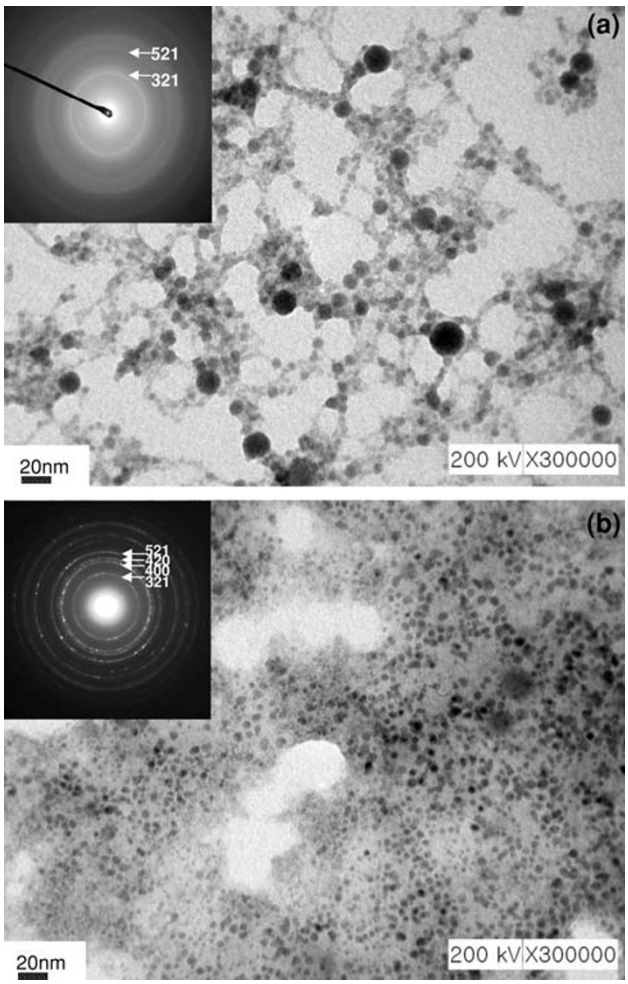

Fig. 3 Typical TEM micrographs of TAG:Ce^{3+} colloidal nanocrystal prepared by PLA in **a** de-ionized water and **b** LDA solution with corresponding electron diffraction patterns

and lattice spacings derived from the diffraction rings were in agreement with the cubic structured TAG:Ce^{3+}.

Figure 4 compares the crystal size distribution of the TAG:Ce^{3+} nanocrystal prepared in (a) de-ionized water and (b) LDA solution by randomly measuring diameters of 160 nanocrystals on the TEM images. Average nanocrystal size in de-ionized water was 11.64 nm with a standard deviation of 7.48 nm. However, TAG:Ce^{3+} nanocrystals prepared in LDA solution exhibited a smaller average size of 6.47 nm and a narrower size distribution of 2.63 nm in standard deviation. Above-mentioned experimental results of XRD, TEM, and size distribution prove that the LDA molecules have important influence on the crystallization and agglomeration process of TAG:Ce^{3+} nanocrystals during the PLA in aqueous media.

The surface composition of the TAG:$Ce^{3\pm}$ nanocrystals prepared in de-ionized water was analyzed using XPS. Figure 5(a–d) presents the high resolution XPS spectra of the Tb 4d (a), Al 2p (b), O 1s (c), and Ce (3d), respectively.

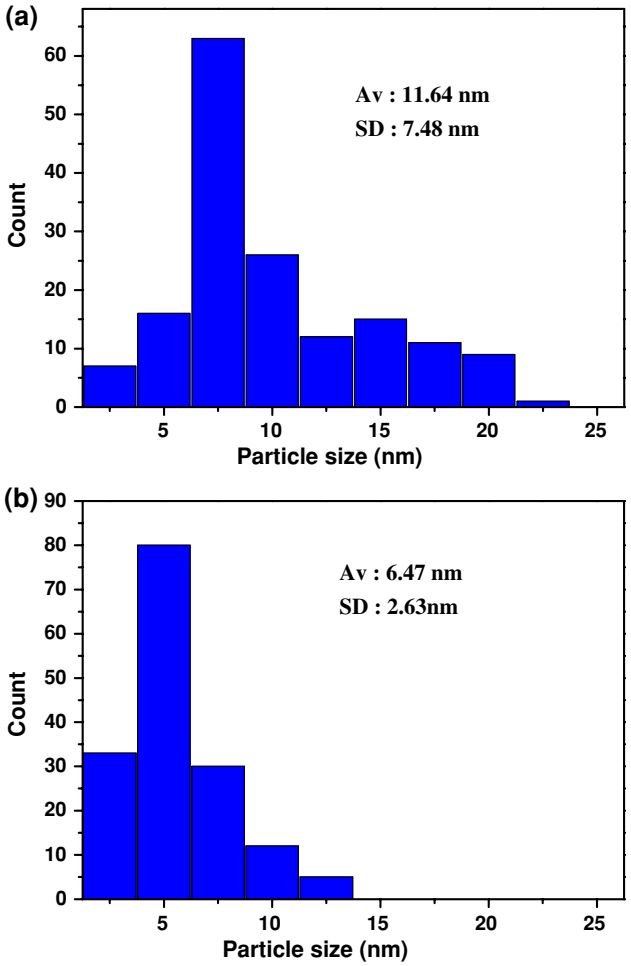

Fig. 4 Size distribution of the prepared TAG:Ce^{3+} colloidal nanocrystals prepared by PLA in **a** de-ionized water and **b** LDA solution. Av and SD denote the average crystallite size and standard deviation value, respectively

The binding energies of the Tb, Al, and O were well in agreement with reported values [21, 22]. The Ce 3d feature in Fig. 5(d) shows a complex structure consisting of Ce $3d_{5/2}$ and Ce $3d_{3/2}$ spin-orbit doublet around 885.6 and 904.4 eV, respectively [23]. The XPS spectra of the TAG:$Ce^{3\pm}$ nanocrystals prepared in LDA solution showed analogous bonding characteristics with prepared in de-ionized water. The calculated chemical compositions of Ce in the TAG:$Ce^{3\pm}$ nanocrystals prepared in de-ionized water and LDA solution were 0.080 and 0.085, respectively, which corresponds well to the doping concentration of bulk target (0.090).

According to previous studies of laser ablation at liquid–solid interfaces [24–26], the initial stage of interaction between the pulsed laser beam and the target surface generates hot-plasma plume over the laser spot on the ceramic target, resulting in intense evaporation from the melt surface, similar to that of PLA in the gas phase or vacuum background. However, because the plasma is confined in the liquid during the laser ablation, it expands outside adiabatically at a supersonic velocity creating shock waves in front, which induces elevated pressure and further increase of plasma temperature. This extremely high transient pressure in the plasma plume can lead to forceful impingement of the ablated species on the confining liquid. In our case, the active species of TAG:Ce^{3+} nanoclusters could strongly react with water molecules at the interfacial region between the plasma and liquid. The initially generated plasma plume is called hot-plasma zone, and the expanded plasma–liquid interfacial region is called reactive quenching zone. This initial cluster served as nuclei and rapidly quenched into the liquid solution together with other radicals or ions such as $OH^{\bullet}$ and H^{+}. It was most likely that the directly quenched cluster of TAG:Ce^{3+} had an amorphous phase due to the transient reaction and rapid quenching. In addition, the quenched clusters in the solution generally had a positively charged surface, because oxygen vacancies were generated easily as a result of the dissociation of oxygen induced by instantaneous high temperature over melting temperature during laser ablation. The pH measurement demonstrated that the liquid solutions were changed from a neutral state (6.8) to a weak acidic state (5.0) after laser ablation.

In the following liquid zone, the surfactant played an important role in the further growth of clusters and inhibition of their aggregation. In de-ionized water, a stable micelle structure on surfaces of the TAG:Ce^{3+} cluster did not form; therefore, seriously agglomerated nanocrystals containing amorphous phase was obtained as shown in Fig. 3(a). However, the LDA molecule, $CH_3(CH_2)_{11}N^+(CH_3)_2CH_2COO^-$, had a local negative charge at the end of its hydrophilic group. Therefore, the LDA molecules surrounded the TAG:Ce^{3+} nanocrystals and formed bilayer-micelles as a result of the electric attractive force between the positive surface of the TAG:Ce^{3+} nanocrystals and the negative charge of the LDA molecules as illustrated in Fig. 6. These bilayer-micelles enabled highly dispersed stable colloidal nanocrystals with reduced surface defects, higher crystallinity, and smaller crystallite size.

Luminescence and Blue-Shift Phenomena of TAG:Ce^{3+} Colloidal Nanocrystals

Figure 7(a, b) depicts the excitation and emission spectra of the TAG:Ce^{3+} colloidal nanocrystals prepared by PLA in de-ionized water and in LDA solution, respectively. The luminescence spectra of the bulk target used for PLA are presented in Fig. 7(c) for comparison with those of nanocrystals. The emission intensities of the nanocrystals prepared in de-ionized water was about 30% of the bulk target. The low emission intensity may be originated from the

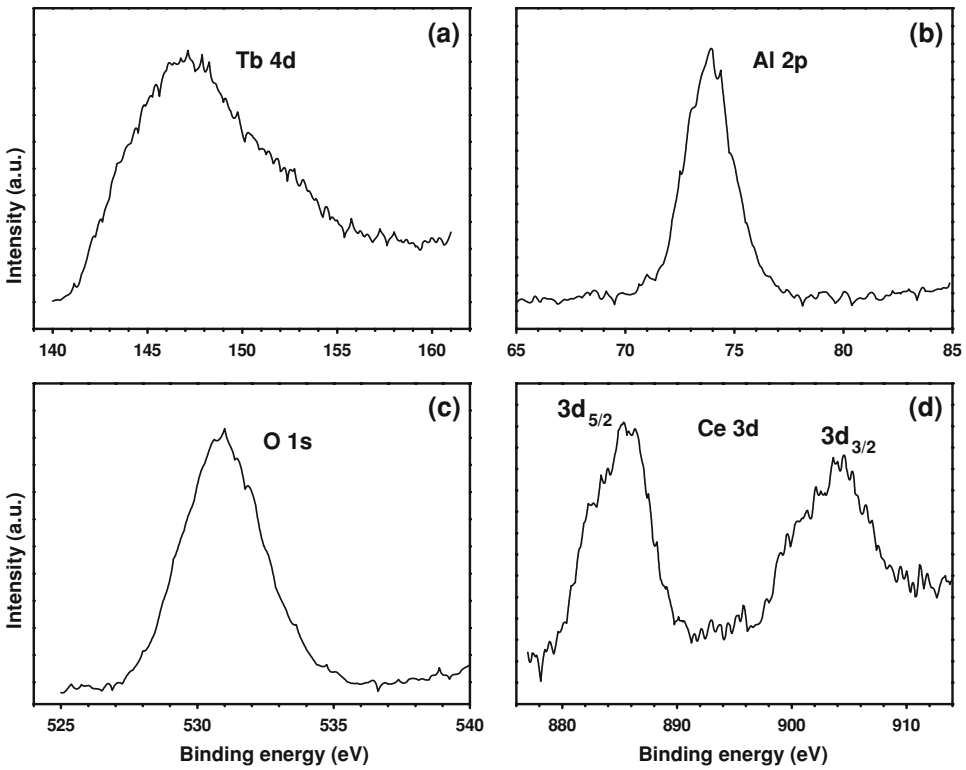

Fig. 5 The XPS spectra of the **a** Tb 4d, **b** Al 2p, **c** O 1s, and **d** Ce 3d region in TAG:Ce^{3+} colloidal nanocrystals prepared in de-ionized water

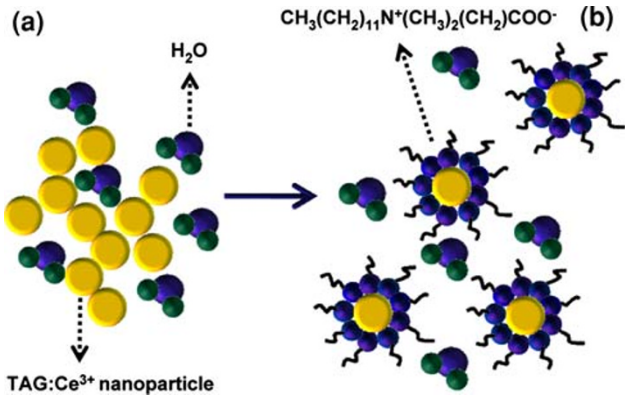

Fig. 6 Schematic diagram describing influence of **a** water and **b** LDA molecules on aggregation process of TAG:Ce^{3+} nanocrystals during PLA in liquid

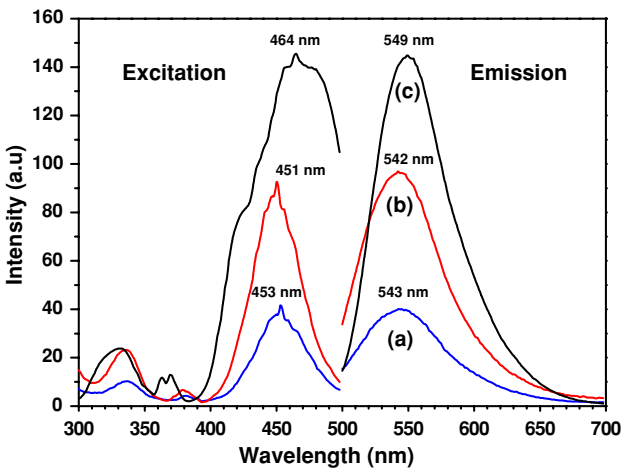

Fig. 7 Excitation and emission spectra of the TAG:Ce^{3+} colloidal nanocrystals prepared in **a** de-ionized water and **b** LDA solution. The PL spectra of bulk target are shown in (**c**) for comparison with those of nanocrystals prepared by PLA

increased nonradiative process in defective surface layer with decrease of crystal size. However, a remarkable enhancement of the emission spectrum up to 70% of the bulk target was observed in the TAG:Ce^{3+} colloidal nanocrystals prepared in LDA solution. This enhancement was not due to the difference in the amount of generated nanocrystals, since the weight of the products was nearly the same for both cases. This result indicated that LDA molecules can passivate surface oxygen defects. LDA is an amphoteric surfactant that possesses a localized negative charge on the oxygen in the carboxyl ion and a localized positive charge on the nitrogen. Therefore, it can be considered that LDA adsorbed on the surface of TAG:Ce^{3+} colloidal nanocrystals can effectively passivate oxygen defect, which is consistent with the explanation for higher crystallinity, better dispersion, and narrower crystallite size distribution.

Moreover, it was clearly observed that the excitation and emission spectra of TAG:Ce^{3+} colloidal nanocrystals were shifted to the blue wavelength region compared to those of the bulk target. There have been many reports [27, 28] on

the blue-shift phenomena in the luminescent spectra of nano-scaled semiconductor materials. However, few reports have focused on nano-sized rare-earth doped phosphor materials. The mechanism of luminescence in the semiconductor is the recombination of electrons in the conduction band and holes in the valence band. A larger band-gap is necessary for quantum confinement to cause the blue-shift in luminescence. However, the luminescence in TAG:Ce^{3+} is due to the transition between energy levels of Ce^{3+} atoms as the luminescence center [8–10]. Therefore, a different interpretation is required to explain the blue-shifts in the luminescence spectra of the TAG:Ce^{3+} nanocrystals.

Figure 8(a) presents a schematic diagram for explanation of blue-shifts in the excitation and emission spectra of TAG:Ce^{3+} nanocrystals. A Ce^{3+} atom has only one electron in 4f orbital, therefore, the electron is excited into a 5d orbital, leaving the 4f shell empty. Based on the energy diagram, the luminescent shift of TAG:Ce^{3+} depends on two parameters of Ce^{3+}: the shift of energy centroid (E_c) in the 5d orbit and the effect of the crystal field splitting (E_{cf}). In Fig. 8(a), the center of gravity (centroid) of the 5d configuration in a polarizable matrix is lower than that in the free ion (4f centroid is zero of energy labeled ΔE_c), and the 5d energy level is split by cubic crystal field into two levels by a gap of 10 Dq.

In the TEM results of Fig. 3, the average particle sizes of prepared TAG:Ce^{3+} colloids were 9.3 nm in de-ionized water and 5.6 nm in LDA solution. Generally, the diminution of crystallite size to nanoscale is closely related with the decrease of the unit cell induced by high surface tension. That is to say, the unit cell of TAG:Ce^{3+} nanocrystals becomes smaller with decrease of crystallite size, which is in accord with the calculated lattice parameters by XRD [29]. According to crystal field theory, the contraction of a unit cell must increase the crystal field around Ce^{3+}, and the greater crystal field splitting energy in the 5d orbital of Ce^{3+} can extend the emission band to longer wavelength [30]. In general, the centroid shift of the 5d configuration is calculated by a ligand polarization model [30, 31] providing values for the spectroscopic polarizability of the anion ligands. In this model, the difference of 5d ↔ 4f centroid changes by the amount

$$\Delta E_c = -\alpha e^2 \left[\langle r^2\rangle_{5d} - \langle r^2\rangle_{4f}\right]/R^6 \quad (1)$$

where $\langle\ \rangle$ denotes the expectation value with respect to the subscript eigenstate, and α is the polarizability of the ligand located at a distance R from Ce^{3+} in a lattice. This model demonstrates the general red-shifting phenomena of rare-earth doped nanocrystalline compounds. These red-shifting phenomena in 4f ↔ 5d transitions have been observed in several Ce^{3+}-doped compounds [32, 33] and interpreted by this crystal field model. However, with this model, it is difficult to interpret the blue-shifting luminescence spectra observed in our TAG:Ce^{3+} colloidal nanocrystal.

In this study, a phenomenological crystal-field model adjusted by the covalency factor [34, 35] was introduced to explain the blue-shift in TAG:Ce^{3+} colloidal nanocrystals. In our model, the crystal field splitting, 10 D_q, includes contributions of the point-charge, lattice-induced dipole, self-induced dipole, and antibonding-overlap term. The antibonding-overlap contribution to 5d energies consisted of antibonding, exchange, and classical overlap; the latter two made the ligand look attractive, therefore giving negative contributions to both 10 D_q and ΔE_c. In predicting the qualitative behavior of the system, it was assumed that net antibonding-overlap contributions to both 10 D_q and ΔE_c were positive. The justification for this assumption was provided by Phillips [36], who argued on general grounds that metal–ligand overlap gives rise to the "nonorthogonality" and "renormalization" terms. These terms lead to an effective repulsion that approximately cancels the classical overlap and exchange. Physically to say, this is Pauli repulsion, since the necessity of orthogonalizing Ψ_a and Ψ_b is a reflection of the Pauli principle as:

$$\Psi_a = (\Phi - S\chi)/(1 - S^2)^{1/2}, \Psi_a = \chi \quad (2)$$

where Φ is a metal orbital, χ is a ligand–complex orbital, and S is the group overlap $<\Phi|\chi>$. The above terms affects the energy eigenvalues of the individual levels and the centroid energy as well. Therefore, the centroid energy and crystal-field splitting energy adjusted by repulsion factor can be written as:

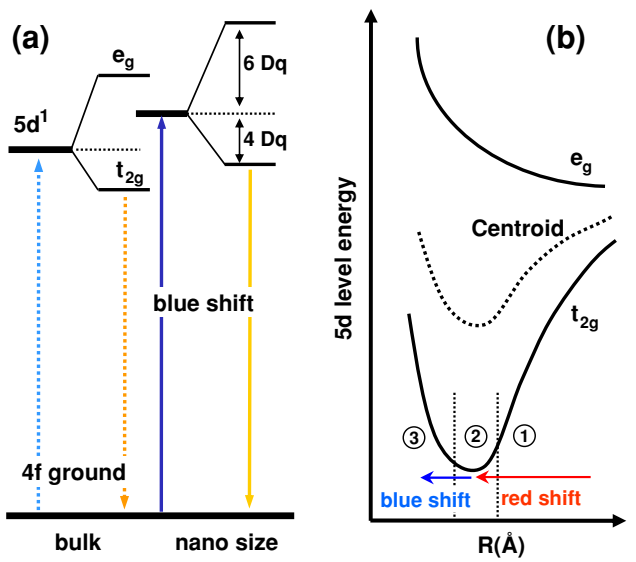

Fig. 8 **a** Schematic diagram for change in Ce^{3+} energy level of TAG:Ce^{3+} nanocrystal and blue-shift in luminescence. **b** Dependence of the 5d energy level of Ce^{3+} on bond distance in a cubic crystal structure

$$10D_q = C_1/R^5 + C_2/R^8 + Ae^{-R/b}, \quad \Delta E_c = -C_3/R^6 + Be^{-R/b} \tag{3}$$

where it is assumed that both π antibonding energy for the t_{2g} level and σ antibonding energy for the e_g level vary exponentially with the nearest-neighbor distance R with the same decay distance b. In effect, C_1, C_2, C_3, A, B, and b are phenomenological parameters adjusted to the measured dependence of 10 Dq and ΔE_c on R in a series of isostructural hosts.

Figure 8(b) depicts the dependence of 5d energy levels and their centroid on bond distance for a cubic structure qualitatively using Eq. (1–3). The range of bond distances in Fig. 8(b) can be divided into three regimes, which are distinguishable in terms of qualitative dependence on the lattice constant. First, in the covalency negligible regime ①, both the t_{2g} level and the 5d centroid decrease as the lattice constant decreases. In the covalency intermediate regime ②, the 5d centroid begins to rise with decreasing lattice constant; the t_{2g} level is near the minimum of the curve as shown in Fig. 8(b), and is therefore insensitive to the lattice constant. It is clear that in the covalency dominant regime ③, the t_{2g} level rises with decreasing lattice constant due to overwhelming antibonding and exclusive effects.

The decrease of bond distance from regimes ① to ② increases the crystal splitting energy and lowers the centroid energy, thus leading the emission band to shift to a longer wavelength (red-shift). However, this phenomena occurring in the range from ① to ② do not seem to be related with the luminescent results of TAG:Ce^{3+} nanocrystals prepared by PLA, because the change of bond distance in regimes ① and ② cannot explain the blue-shifted luminescence observed in prepared TAG:Ce^{3+} colloidal nanocrystals. Therefore, it can be concluded that the bond distance of the Ce^{3+} in TAG decreased from regime ② into ③ as the crystal size decreased to nanoscale, and induced the rising of centroid and t_{2g} energy levels. Consequently, the changes of energy levels in the centroid and t_{2g} shifted excitation and emission spectra to a shorter wavelength as confirmed in Fig. 7. In the synthesis section, we revealed that the TAG:Ce^{3+} colloidal nanocrystal prepared in LDA solution had smaller average crystallite size and a narrower size distribution than those prepared in de-ionized water. Therefore, blue-shift into shorter wavelength in luminescence of the TAG:Ce^{3+} colloidal nanocrystals prepared in LDA solution compared to those prepared in de-ionized water, and bulk target can be explained well by this modified crystal field model.

Conclusion

TAG:Ce^{3+} colloidal nanocrystals were fabricated by an one-step simple route using PLA in de-ionized water and LDA solution for luminescent bio-labeling application. In LDA solution, the crystallite size and the standard deviation of crystallite size decreased, whereas emission intensity increased remarkably. This result indicated that anionic oxygen in the LDA molecules effectively occupied the oxygen vacancy sites on the surface of TAG:Ce^{3+} colloidal nanocrystal by the charge matching with the positively charged colloidal nanocrystals. The origin of blue-shift in luminescence spectra was investigated in detail by a phenomenological model based on the covalency contribution to the crystal field splitting energy of Ce^{3+} with decreasing of bond length. It is worthy that this is a new account of room-temperature synthesis of TAG:Ce^{3+} colloidal nanocrystal using PLA in liquid media. Furthermore, the experimental evidences of blue-shifts in luminescence spectra can be helpful in understanding the nano-size effect on the 5d energy level of Ce^{3+}-doped compounds.

References

1. G. Ocvirk, T. Tang, D.J. Harrison, Analyst **123**, 1429–1434 (1998)
2. A.T. Woolley, K. Lao, A.N. Glazer, R.A. Mathies, Anal. Chem. **70**, 684–688 (1998)
3. D. Maxwell, J. Taylor, S. Nie, J. Am. Chem. Soc. **124**, 9606–9612 (2002)
4. I.L. Medintz, H.T. Uyeda, E.R. Goldman, H. Mattoussi, Nat. Mater. **4**, 435–446 (2005)
5. J. Zhang, R.E. Capbell, A.Y. Ting, R.Y. Tsien, Nat. Rev. Mol. Cell Biol. **3**, 906–918 (2002)
6. F. Wang, W.B. Tan, Y. Zhang, Z. Fan, M. Wang, Nanotechnology **17**, R1–R3 (2006)
7. B. Sun, G. Yi, D. Chen, Y. Zhou, J. Cheng, J. Mater. Chem. **12**, 1194–1198 (2002)
8. M. Nazarov, D.Y. Noh, J.R. Sohn, C.S. Yoon, J. Solid State Chem. **180**, 2493–2499 (2007)
9. Y. Chen, J. Wang, M. Gong, Q. Su, J. Solid State Chem. **180**, 1165–1170 (2007)
10. C.C. Chiang, M.S. Tsai, M.H. Hon, J. Alloys Comp. **431**, 298–302 (2007)
11. J. Heddersen, G. Chumanov, T.M. Cotton, Appl. Spectrosc. **47**, 1959–1964 (1993)
12. J.B. Wang, G.W. Yang, C.Y. Zhang, X.L. Zhong, Z.H.A. Ren, Chem. Phys. Lett. **367**, 10–14 (2003)
13. F. Mafuné, J. Kohno, Y. Takeda, T. Kondow, H. Sawabe, J. Phys. Chem. B **105**, 5114–5120 (2001)
14. R. Kumar, A.K. Shukla, H.S. Mavi, V.D. Vankar, Nanoscale Res. Lett. **3**, 105–108 (2008)
15. S.-R. Jian, I.-J. Teng, P.-F. Yang, Y.-S. Lai, J.-M. Lu, J.-G. Chang, S.-P. Ju, Nanoscale Res. Lett. **3**, 186–193 (2008)
16. B.W. Mwakikunga, A. Forbes, E.S. Haddad, C. Arendse, Nanoscale Res. Lett. **3**, 372–380 (2008)
17. G.S. Park, K.M. Kim, S.W. Mhin, J.W. Eun, K.B. Shim, J.H. Ryu, N. Koshizaki, Electrochem. Solid-State Lett. **11**, J23–J26 (2008)
18. S. Zhou, Z. Fu, J. Zhang, S. Zhang, J. Lumin. **118**, (2006) 179–185

19. K.M. Kim, J.H. Ryu, S.W. Mhin, G.S. Park, K.B. Shim, J. Electrochem. Soc. **155**, J293–J296 (2008)
20. H. Usui, Y. Shimizu, T. Sasaki, N. Koshizaki, J. Phys. Chem. B **109**, 120–124 (2005)
21. M. Kruczek, E. Talik, H. Sakowska, M. Gała, M. Świrkowicz, Cryst. Res. Technol. **40**, 439–443 (2005)
22. B.M. Reddy, P. Saikia, P. Bharali, Y. Yamada, T. Kobayashi, M. Muhler, W. Grünert, J. Phys. Chem. C **112**, 16393–16399 (2008)
23. S. Giuffrida, G.G. Condorelli, L.L. Costanzo, G. Ventimiglia, A.D. Mauro, I.L. Fragalà, J. Photochem. Photobiol. A **195**, 215–222 (2008)
24. V.V. Ageev, A.F. Bokhonov, V.V. Zhukovskii, A.A. Yankovskii, J. Appl. Spectr. **64**, 668–674 (1997)
25. T. Sakka, S. Iwanaga, Y.H. Ogata, A. Matsunawa, T. Takemoto, J. Chem. Phys. **112**, 8645–8653 (2000)
26. Y.H. Chen, C.H. Yeh, Colloid Surf. A **197**, 133–139 (2002)
27. A.D. Yoffe, Adv. Phys. **42**, 173–266 (1993)
28. A. D'Andrea, R. Del Sole, Solid State Commun. **74**, 1121–1124 (1990)
29. Q. Li, L. Gao, D. Yan, Mater. Chem. Phys. **64**, 41–44 (2000)
30. P. Dorenbos, Phys. Rev. B **65**, 235110 (2002)
31. Y. Pan, M. Wu, Q. Su, J. Phys. Chem. Solids **65**, 845–850 (2004)
32. M. Nazarov, C. Yoon, J. Solid. State Chem. **179**, 2529–2533 (2006)
33. K. Li, G. Shucai, H. Guangyan, Z. Jilin, J. Rare Earth **25**, 692–696 (2007)
34. B.F. Aull, H.P. Jenssen, Phys. Rev. B **34**, 6640–6646 (1986)
35. B.F. Aull, H.P. Jenssen, Phys. Rev. B **34**, 6647–6655 (1986)
36. J.C. Phillips, J. Phys. Chem. Solid **11**, 226–230 (1959)